Journal of Applied Polymer Science

Effects of Emulsion Parameters on Relaxation Behaviors for Immiscible Polymer Blends

Lin-Qiong Xu, Han-Xiong Huang, Zhao-Ke Chen, Xiong-Jun Wu

Lab for Micro Molding and Polymer Rheology, The Key Laboratory of Polymer Processing Engineering of the Ministry of Education, Department of Industrial Equipment and Control Engineering, South China University of Technology, Guangzhou 510640, People's Republic of China

Correspondence to: H.-X. Huang (E-mail: mmhuang@scut.edu.cn)

ABSTRACT: The relaxation behaviors of the binary immiscible blends reflected on the plots of the storage modulus and the imaginary part of complex viscosity were investigated using the Maxwell and the Palierne models. It was revealed that the peaks in the high- and low-frequency regions on the complex viscosity imaginary part plot are owing to the relaxations of the blend and deformed dispersed droplets, respectively. Based on these two models, six emulsion parameters (interfacial tension, relaxation times and viscosities of two components, and dispersed phase volume fraction) were investigated in terms of their effects on the shape features of the plots of the imaginary part of complex viscosity and the Cole–Cole. The results showed that the viscosities of two components and dispersed phase volume fraction play key roles in the radii of the two circular arcs on the Cole–Cole plot. Furthermore, the two circular arcs are well separated in the case of lower interfacial tensions and dispersed phase viscosities, shorter matrix relaxation times, and higher matrix viscosities and dispersed phase volume fractions. The total relaxation time of the deformed dispersed droplets increases with increasing the viscosities of two components, especially with decreasing the interfacial tension. Three types of polymer blends were prepared and their dynamic frequency sweep testing results demonstrated the effectiveness of the corresponding predicted results. © 2013 Wiley Periodicals, Inc. J. Appl. Polym. Sci. **2014**, *131*, 39690.

KEYWORDS: blends; extrusion; rheology; viscosity; viscoelasticity

Received 9 January 2013; accepted 19 June 2013

DOI: 10.1002/app.39690

INTRODUCTION

The relaxation behaviors of the immiscible polymer blends may give useful information on their interfacial properties and phase morphologies.[1–6] The rheological functions, such as the storage modulus,[1–3,5] loss tangent,[7] and Cole–Cole plots[4,8–11] can reflect the relaxation behaviors of the blends. There exist two relaxation processes for the immiscible blends in the whole tested frequency range. The one is for the relaxation of the blends; the other for the relaxation of the deformed dispersed droplets in the matrix, that is, the second relaxation mechanism for the blends. The latter relaxation process leads to higher elasticity of the blend compared with those of the pure components in the blend, which is reflected on the storage modulus and loss tangent plots in the low frequency region.[2,7,11] Moreover, it results in the appearance of a tail or even a circular arc in the low frequency region on the Cole–Cole plot.[8–11] Several researchers have used these phenomena to analyze the miscibility of the polymer blends[9–13] and predict the phase inversion composition.[9,14] To the best knowledge of the authors, few researchers have ever reported the influencing factors on the Cole–Cole plots for the immiscible blends. Graebling et al.[2] investigated the effects of the matrix relaxation time and droplet size distribution at constant volume average radius of the dispersed droplets on the Cole–Cole plots for the immiscible blends. The results showed that the two circular arcs on the Cole–Cole plot are well separated at short matrix relaxation times. However, the droplet size distribution has little influence on the Cole–Cole plot. Recently, Wu et al.[10] reported that the addition of the copolymers into the poly(ε-caprolactone)/poly(lactic acid) (PCL/PLA) blends reduces the interfacial tension between the two components, and thus the circular arcs of the Cole-Cole plot shift up to low frequency region. Li et al.[14] investigated the rheological properties for the PLA/poly(butylenes adipate-*co*-terephthalate) (PBAT) blends with 5–80 wt % PBAT. For the Cole–Cole plot, the 80/20 PLA/PBAT blend presents two circular arcs, whereas the 70/30 and 50/50 blends only show a tail in the low frequency region.

Several rheological models have been proposed to describe the viscoelasticity of the immiscible blends with droplet-matrix morphology[1,2,15] and cocontinuous structure.[16] The Palierne model[1,2] is one of the most widely used models to describe the

Table I. Characteristic Properties and Manufacturers of PP, PLA, PBS, and LLDPE Used in This Work

Material	Manufacturer	Grade	MFI (g/10 min)	Density (g cm^{-3})	Zero-shear viscosity (Pa s^{-1})
PP	Sinopec Guangzhou Group	J501	2.7 (230°C, 2.16 kg)	0.91	8898
PLA	NatureWorks® LLC	2002D	8.8 (210°C, 2.16 kg)	1.24	2957
PBS-1	Xinfu Pharmaceutical Co., Ltd	1903I	15.3 (150°C, 2.16 kg)	1.24	559
PBS-2	Xinfu Pharmaceutical Co., Ltd	1903F	5 (150°C, 2.16 kg)	1.18	679
LLDPE	Sinopec Maoming Company	DFDA-7072	2 (190°C, 2.16 kg)	0.92	6712

viscoelasticity of the binary immiscible blends with droplet-matrix morphology. This model is a constitutive equation for the complex modulus as a function of the interfacial tension, dispersed phase volume fraction, average dispersed phase radius, and component complex moduli. Among them, the complex moduli of the components are dependent on the their zero-shear viscosities and relaxation times according to the Maxwell model.[17]

For the aforementioned reasons, this work aimed at investigating the influencing factors of the Cole–Cole plot for the binary immiscible blends with droplet-matrix morphology based on the Maxwell[17] and the Palierne[1,2] models. Six emulsion parameters, that is, the interfacial tension between two components, relaxation times and viscosities of two components, and dispersed phase volume fraction, were taken into account at constant average radius of the dispersed phase. Their influencing mechanisms were investigated in terms of the relaxation behaviors reflected on the plots of the storage modulus and the imaginary part of complex viscosity. Moreover, some predicted results were confirmed by the experimental results for three types of polymer blends.

THEORETICAL MODEL

In this work, the complex moduli of the matrix, dispersed phase, and blend were calculated based on the Maxwell[17] and the Palierne[1,2] models, which are written as follows:

$$G_m^*(\omega)=\frac{i\omega\eta_m}{1+i\omega\lambda_m} \tag{1}$$

$$G_i^*(\omega)=\frac{i\omega\eta_i}{1+i\omega\lambda_i} \tag{2}$$

$$G_b^*(\omega)=G_m^*(\omega)\frac{1+3\varphi H(\omega)}{1-2\varphi H(\omega)} \tag{3}$$

where

$$H(\omega)=\frac{4\frac{\alpha}{R_V}[2G_m^*(\omega)+5G_i^*(\omega)]+[G_i^*(\ \omega\ )-G_m^*(\omega)][16G_m^*(\omega)+19G_i^*(\omega)]}{40\frac{\alpha}{R_V}[G_m^*(\omega)+G_i^*(\omega)]+[2G_i^*(\omega)+3G_m^*(\omega)][16G_m^*(\omega)+19G_i^*(\omega)]} \tag{4}$$

and G_m^*, G_i^* and, G_b^* are the complex moduli of the matrix, dispersed phase, and blend, respectively; η_m and η_i are the zero-shear viscosities of the matrix and dispersed phase, respectively; λ_m and λ_i are the relaxation times of the matrix and dispersed phase, respectively; ω is the angle frequency; α is the interfacial tension between two components of the blend; φ and R_V are the volume fraction and volume average radius of the dispersed phase.

Giving the values of the η_m, λ_m, η_i, and λ_i, the $G_m^*(\omega)$ and $G_i^*(\omega)$ were calculated using eqs. (1) and (2), respectively. The $G_b^*(\omega)$ was obtained by substituting the calculated values of the $G_m^*(\omega)$ and $G_i^*(\omega)$ into eq. (3) at the given values of the α, φ, and R_V. Then, the storage (G') and loss (G'') moduli of the matrix, dispersed phase, and blend were determined based on the following equation:

$$G^*=G'+iG'' \tag{5}$$

Finally, the imaginary part η'' ($=G'/\omega$) and real part η' ($=G''/\omega$) of the complex viscosities (η^*) of the matrix, dispersed phase, and blend were calculated.

EXPERIMENTAL

Materials and Sample Preparation

In this work, four kinds of materials were used: polypropylene (PP), PLA, poly(butylene succinate) (PBS), and linear low-density polyethylene (LLDPE). The manufacturers, grades, melt flow indices (MFI), densities, and zero-shear viscosities of the used materials are listed in Table I. Two PBS grades were chosen: 1903I (injection molding grade, denoted as PBS-1) and 1903F (film grade, denoted as PBS-2).

Three types of polymer blends were prepared using a single-screw extruder: 70/30 and 80/20 (w/w) PLA/LLDPE, 80/20 (w/w) PLA/PBS-1, and 85/15 (w/w) PBS-2/PP blends. The PLA/LLDPE blends with 20 and 30 wt % LLDPE were used to investigate the effect of the dispersed phase volume fraction on the Cole–Cole and $\eta''(\omega)$ plots. The PLA/LLDPE and PLA/PBS blends with the same weight fraction (20 wt %) were used to investigate the effect of the dispersed phase viscosity on the two plots. The PBS-2/PP blend with a viscosity ratio of 13.1 was used to analyze the two plots for the blend with low matrix viscosity. The used extruder screw was equipped with special screw

elements, which can provide good mixing under lower shear intensity,[18–20] and so are favorable to the processing of the biodegradable polyesters. The extruder barrel temperatures from the hopper to the die were 160–180–180–180°C. The screw speed and feeding rate were set at 40 rpm and 3 kg h^{-1}, respectively. For comparison, the used four kinds of materials were also processed under the same conditions. The as-extruded blend rods were collected from the die exit and quenched in iced water as soon as possible to preserve the blend morphology at the die exit. The disks with a diameter of 25 mm and a thickness of about 1.5 mm were immediately compressed from the melt just out of the die exit and quenched in iced water quickly. Then, all the prepared samples were dried at 60°C for 4 h in a vacuum oven.

Characterization

Bohlin Gemini 200 Rheometer (Bohlin, Worcestershire, UK) equipped with a parallel-plate fixture (25 mm diameter) was used in an oscillatory mode to conduct dynamic frequency sweep tests on the previously prepared disks of the blends and used four kinds of materials. The η^*, G', and G'' as a function of ω ranging from 0.0628 to 628 rad s^{-1} were measured at 180°C. A fixed strain of 5% was used to ensure that the measurements were carried out within the linear viscoelastic range of the materials and blend samples investigated. From the $\eta^*(\omega)$ plots of the used materials, their zero-shear viscosities were obtained and are listed in Table I.

The previously prepared blend rods were immersed in liquid nitrogen for about 10 min and fractured along the melt-flow direction. Then they were gold sputtered and their cryo-fractured surfaces were examined using SEM (Quanta 200, FEI, Eindhoven, Holland) at an accelerating voltage of 15 kV. The results show that all as-extruded blends exhibit droplet-matrix morphology. The volume and number average radii (R_V, R_n) of the dispersed droplets were estimated by:

$$R_V = \frac{\sum_i n_i R_i^4}{\sum_i n_i R_i^3} \tag{6}$$

$$R_n = \frac{\sum_i n_i R_i}{\sum_i n_i} \tag{7}$$

where R_i is the radius of each droplet and n_i is the number of droplets with R_i. The R_V, R_n, and R_V/R_n of the dispersed droplets in as-extruded blends were obtained by analyzing the SEM micrographs (not shown here) of the as-extruded blends, and the results are listed in Table II. As can be seen, all the values of the R_V/R_n meet the condition for the application of the Palierne model, that is, the polydispersity does not exceed a value of about 2.3.

RESULTS AND DISCUSSION

In the following, the aforementioned calculated methods were used to obtain the $G'(\omega)$ and $\eta''(\omega)$ plots for a given binary immiscible blends. Their relaxation behaviors reflected on the two plots were analyzed. Then, six emulsion parameters were investigated in terms of their effects on the shape features of the Cole–Cole and $\eta''(\omega)$ plots of the blends. In addition, some predicted results were confirmed by the experimental results for three types of polymer blends.

Table II. R_V, R_n, and R_V/R_n of Dispersed Droplets for As-Extruded PLA/LLDPE, PLA/PBS-1, and PBS-2/PP Blends

Blend	R_V (μm)	R_n (μm)	R_V/R_n
70/30 (w/w) PLA/LLDPE blend	3.80	2.65	1.43
80/20 (w/w) PLA/LLDPE blend	3.66	2.42	1.51
80/20 (w/w) PLA/PBS-1 blend	0.64	0.32	2.00
85/15 (w/w) PBS-2/PP blend	12.44	6.20	2.01

Relaxation Behaviors Reflected on Plots of Storage Modulus and Complex Viscosity Imaginary Part

Figure 1 shows the $G'(\omega)$ and $\eta''(\omega)$ plots of a typical immiscible blend, which were obtained by setting the six emulsion parameters as follows: $\eta_m = 10^4$ Pa s^{-1}, $\eta_i = 5 \times 10^3$ Pa s^{-1}, $\lambda_m = \lambda_i = 0.1$ s, $\varphi = 0.2$, and $\alpha/R_V = 5000$ Pa. It can be clearly seen that there is a secondary plateau on the $G'(\omega)$ plot. According to the definitions by Graebling et al.,[2] there exist three relaxation times on the $G'(\omega)$ plot for the blend, that is, λ_M, λ_P, and λ_D. These relaxation times were calculated using equations proposed by Graebling et al.[2] and the results are displayed in Figure 1. Among them, λ_M is the mean relaxation time of the blend, λ_P is the time corresponding to the beginning of the relaxation of the dispersed droplets, and λ_D is the longest relaxation time of the blend and corresponds to the total shape relaxation of the dispersed droplets. That is, there exist two relaxation processes for the blend in the whole tested frequency range: the one is for the relaxation of the blend, and the other for the relaxation of the deformed dispersed droplets.

The aforementioned two relaxation processes lead to two peaks and a depression on the $\eta''(\omega)$ plot, as shown in Figure 1. The reciprocals of the frequencies corresponding to the peak in the

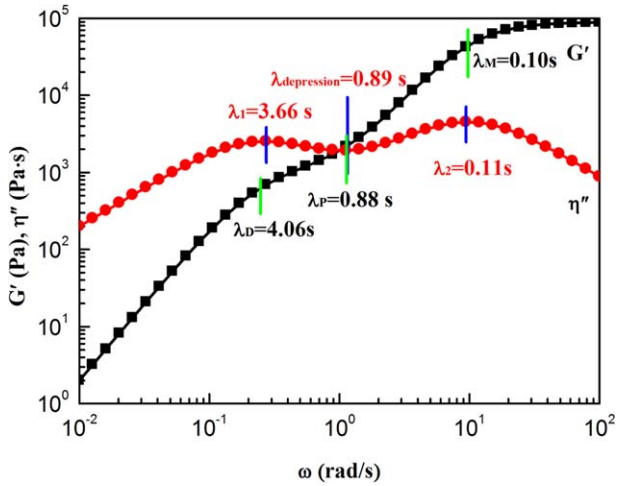

Figure 1. $G'(\omega)$ and $\eta''(\omega)$ plots for typical immiscible blend. [Color figure can be viewed in the online issue, which is available at wileyonlinelibrary.com.]

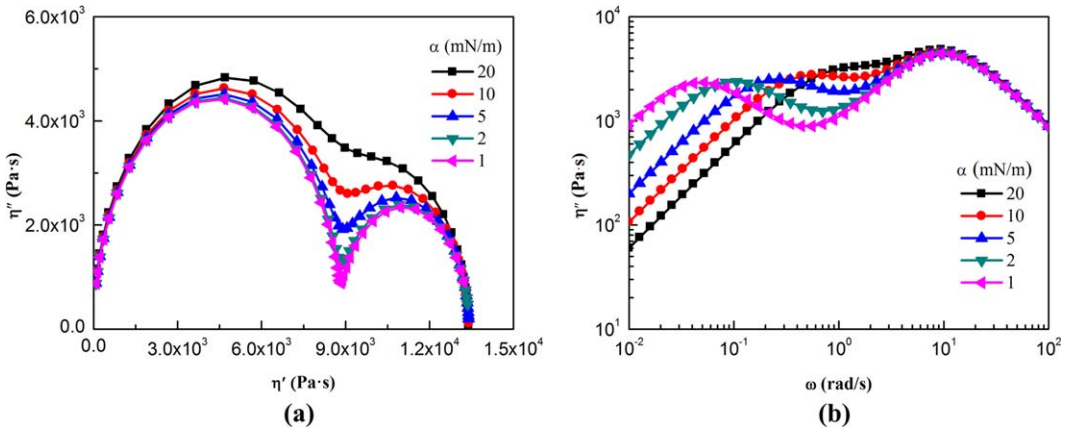

Figure 2. Effect of interfacial tension on (a) Cole–Cole and (b) $\eta''(\omega)$ plots of blends. [Color figure can be viewed in the online issue, which is available at wileyonlinelibrary.com.]

low frequency region, to the depression, and to the peak in the high frequency region on the $\eta''(\omega)$ plot for the binary immiscible blend are defined as its characteristic relaxation times, and denoted as λ_1, $\lambda_{\text{depression}}$, and λ_2, respectively. It can be clearly seen from Figure 1 that the values of the λ_1, $\lambda_{\text{depression}}$, and λ_2 are very close to those of the λ_D, λ_P, and λ_M, respectively. This indicates that the peak in the low frequency region on the $\eta''(\omega)$ plot is owing to the relaxation of the deformed dispersed droplets, and the λ_1, $\lambda_{\text{depression}}$, and λ_2 have the same physical significance as the λ_D, λ_P, and λ_M, respectively. As can be also seen in Figure 1, the shape feature reflecting the relaxation behavior on the $\eta''(\omega)$ plot is more distinct than that on the $G'(\omega)$ plot. Moreover, the λ_1, $\lambda_{\text{depression}}$, and λ_2 on the $\eta''(\omega)$ plot can be obtained from the plot directly, whereas the λ_D, λ_P, and λ_M on the $G'(\omega)$ plot should be calculated using the equations proposed by Graebling et al.[2] That is, the former three relaxation times are more convenient to be obtained than the latter ones.

Influences of Emulsion Parameters on Plots of Cole–Cole and Complex Viscosity Imaginary Part

The aforementioned six emulsion parameters are investigated in terms of their effects on the shape features of the Cole–Cole and $\eta''(\omega)$ plots of the blends. The values of the six parameters are set in the common regions for the polymer materials as follows: α = 0–20 mN m^{-1}, λ_i = 0.05–0.5 s, λ_m = 0.05–0.5 s, $\eta_i = 1 \times 10^3$–2.5×10^4 Pa s^{-1}, $\eta_m = 1 \times 10^3$–1×10^4 Pa s^{-1}, φ = 0.1–0.4. As investigating the effect of one parameter, other parameter values are kept constant as follows: $\eta_m = 10^4$ Pa s^{-1}, $\eta_i = 5 \times 10^3$ Pa s^{-1}, $\lambda_m = \lambda_i = 0.1$ s, $\varphi = 0.2$, and $\alpha = 5$ mN m^{-1}. The R_V is always set at 1 μm.

Figure 2 shows the influence of the α between the two phases on the Cole–Cole and $\eta''(\omega)$ plots of the blends. From Figure 2(a), it can be seen that the two circular arcs exhibit more distinct separation with decreasing the α, whereas the α has little effect on the radii of the two circular arcs. From Figure 2(b), the three relaxation times (λ_1, $\lambda_{\text{depression}}$, and λ_2) of the blends are obtained according to their definitions mentioned above and the results are listed in Table III, in which the λ_D, λ_P, and λ_M calculated using the Palierne model[1,2] are also given. As can be clearly observed, for every value of the α, the values of the λ_1, $\lambda_{\text{depression}}$, and λ_2 are very close to those of the λ_D, λ_P, and λ_M, respectively. With the decrease in the α, the $\lambda_{\text{depression}}$ steadily increases, whereas the λ_1 exhibits a sharp increase. This is attributed to the fact that the decrease in the α leads to stronger interaction between the phases, retarding the relaxation of the deformed dispersed droplets. According to the equation for calculating the λ_M,[2] its values are independent on the α, and the λ_2 obtained from the $\eta''(\omega)$ plots at different values of α also has the same value (as shown in Table III).

As may be expected, the λ_i and λ_m play roles in the Cole–Cole and $\eta''(\omega)$ plots of the blends. Figures 3 and 4 illustrate the influences of the λ_i and λ_m on the two plots, respectively. Comparing Figure 3 with Figure 4 shows that on the whole, the λ_i has almost no effect, whereas the λ_m has a great impact on the shapes of the two plots. The lower the value of λ_m, the more obviously the two circular arcs of the Cole–Cole plot are separated. As shown in Figure 4(b), with increasing the λ_m, the frequencies corresponding to the peak in the high frequency region and depression gradually move toward lower values, that is, the λ_2 and $\lambda_{\text{depression}}$ increase. Furthermore, the peak in the high frequency region is gradually close to that in the low frequency region, which induces the two circular arcs to be separated poorly.

As mentioned above, the α, λ_i, and λ_m have little effect on the radii of the two circular arcs of the Cole–Cole plots of the

Table III. Relaxation Times Obtained from $\eta''(\omega)$ Plots and Calculated Using the Palierne Model at Different α

α (mN m^{-1})	20	10	5	2	1
λ_1 (s)	—	1.80	3.66	9.43	19.15
λ_D (s)	1.01	2.03	4.06	10.14	20.28
$\lambda_{\text{depression}}$ (s)	—	0.49	0.89	1.42	1.80
λ_P (s)	0.44	0.62	0.88	1.39	1.97
λ_2 (s)	0.11	0.11	0.11	0.11	0.11
λ_M (s)	0.10	0.10	0.10	0.10	0.10

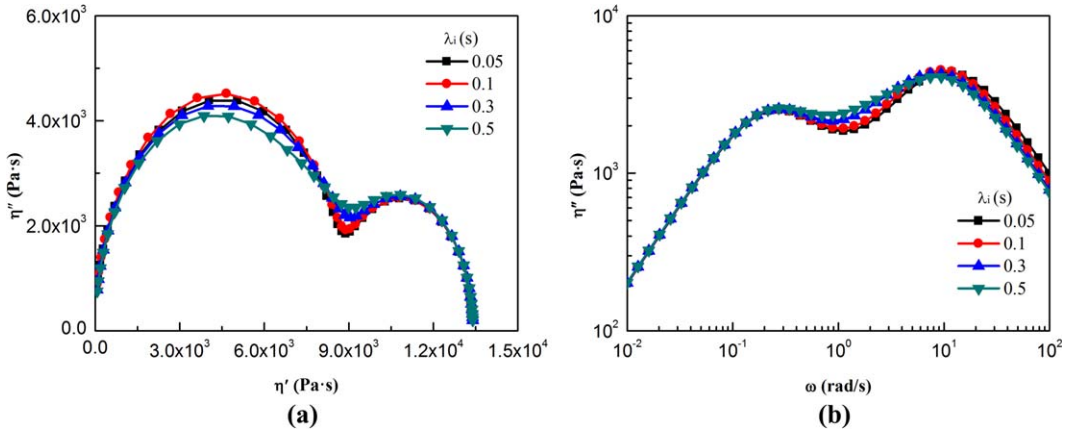

Figure 3. Effect of relaxation time of dispersed phase on (a) Cole–Cole and (b) $\eta''(\omega)$ plots of blends. [Color figure can be viewed in the online issue, which is available at wileyonlinelibrary.com.]

blends at constant value of R_V [as shown in Figures 2(a), 3(a), and 4(a)]. Now the influences of the η_i and η_m on the Cole–Cole and $\eta''(\omega)$ plots of the blends are investigated, and the results are shown in Figures 5 and 6. As can be seen from Figures 5(a) and 6(a) that with increasing the η_i or η_m, the radius of the circular arc in the high frequency region becomes larger,

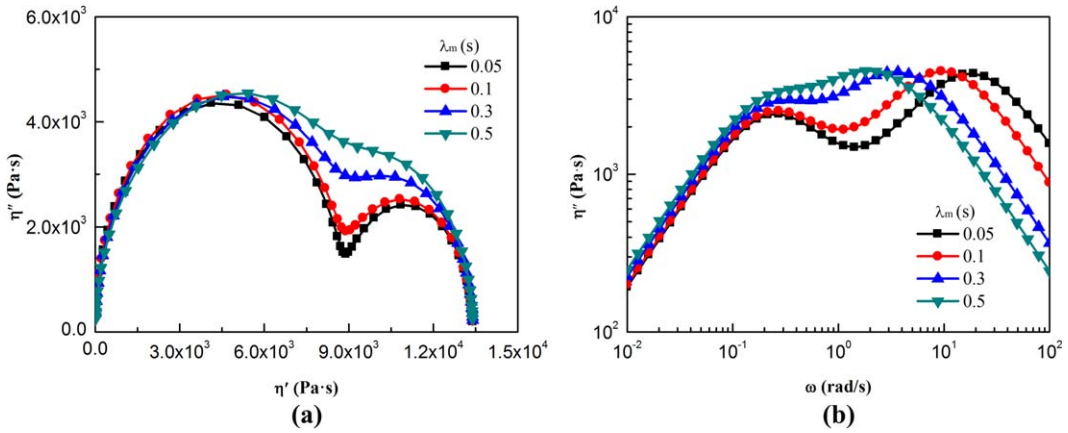

Figure 4. Effect of relaxation time of matrix on (a) Cole–Cole and (b) $\eta''(\omega)$ plots of blends. [Color figure can be viewed in the online issue, which is available at wileyonlinelibrary.com.]

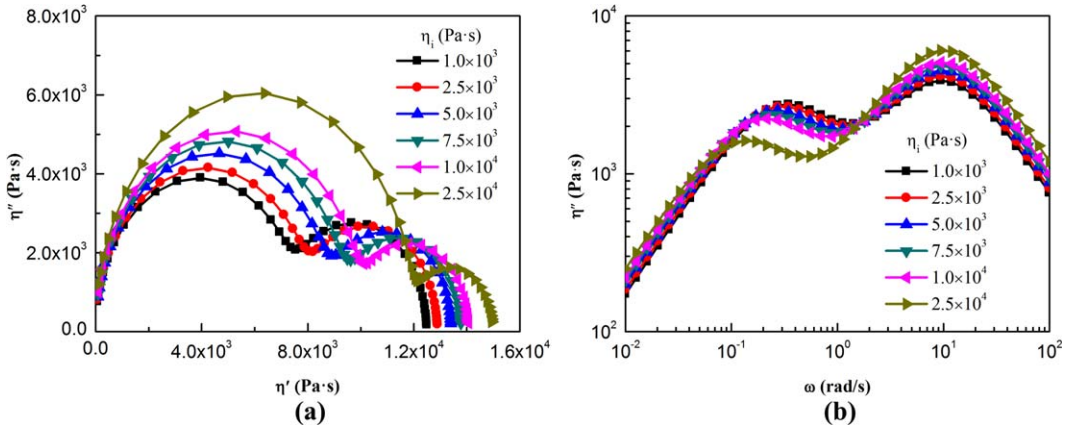

Figure 5. Effect of dispersed phase viscosity on (a) Cole–Cole and (b) $\eta''(\omega)$ plots of blends. [Color figure can be viewed in the online issue, which is available at wileyonlinelibrary.com.]

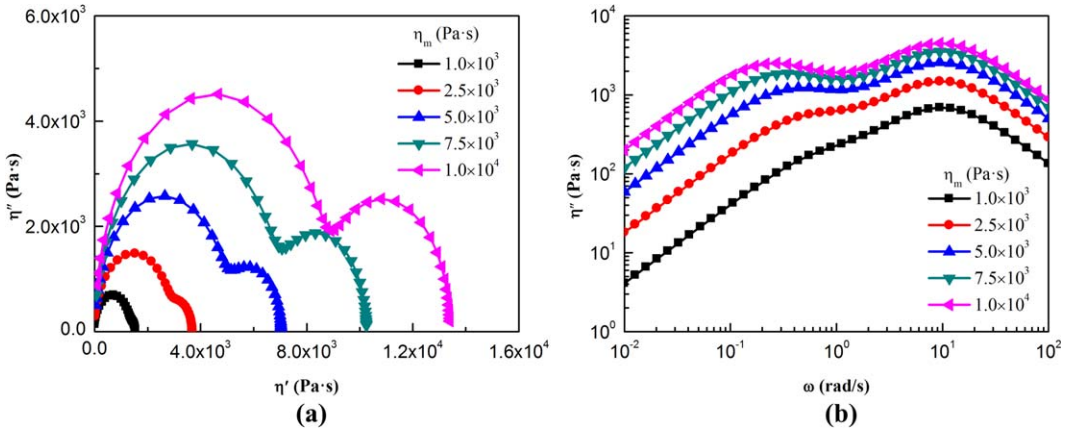

Figure 6. Effect of matrix viscosity on (a) Cole–Cole and (b) $\eta''(\omega)$ plots of blends. [Color figure can be viewed in the online issue, which is available at wileyonlinelibrary.com.]

whereas the radius in the low frequency region becomes smaller and larger, respectively. Increasing the η_m or decreasing the η_i leads to well separation of the two circular arcs of the Cole–Cole plot. Specially, there is no peak on the circular arc in the low frequency when the value of the η_m is lower than 2.5×10^3 Pa s^{-1}. These can be explained briefly as follows. The circular arcs in the high- and low-frequency regions on the Cole–Cole plot are owing to the relaxations of the blend and deformed

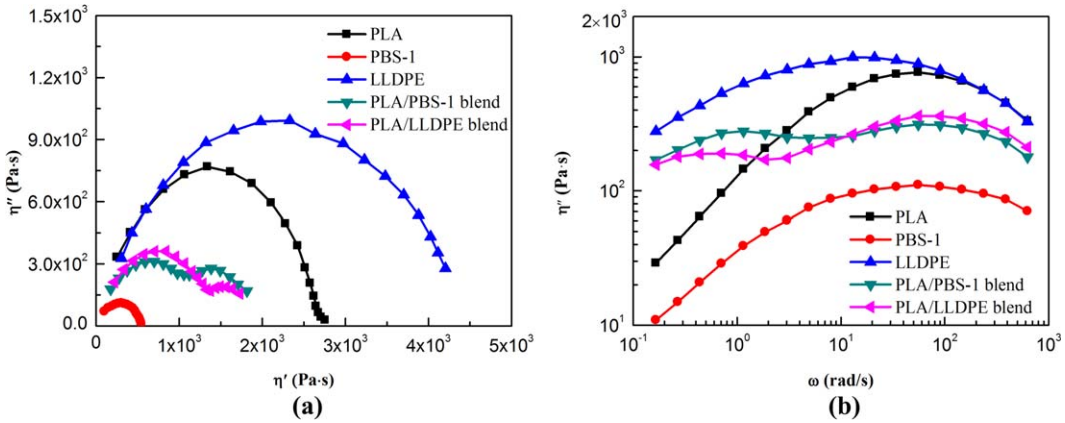

Figure 7. (a) Cole–Cole and (b) $\eta''(\omega)$ plots of as-extruded 80/20 (w/w) PLA/PBS-1 (η_r = 0.19) and PLA/LLDPE (η_r = 2.27) blends and pure PLA, PBS-1, and LLDPE. [Color figure can be viewed in the online issue, which is available at wileyonlinelibrary.com.]

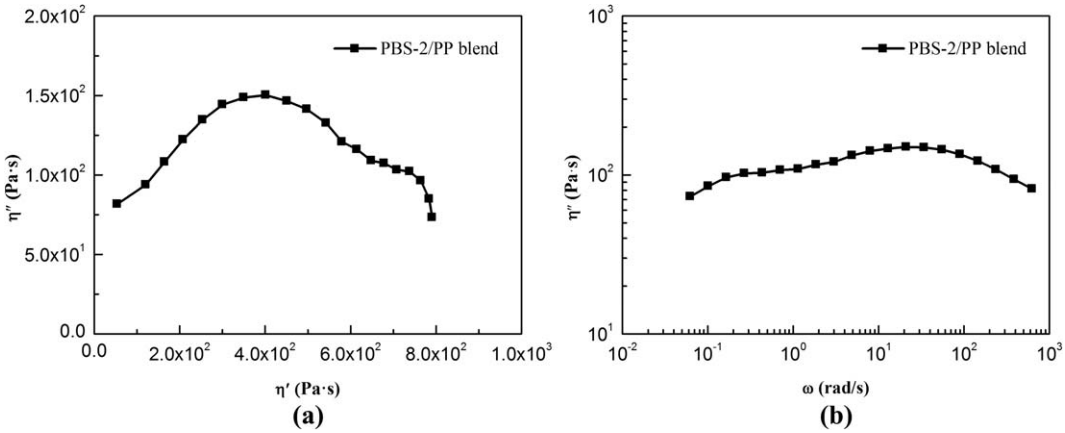

Figure 8. (a) Cole–Cole and (b) $\eta''(\omega)$ plots of as-extruded 85/15 (w/w) PBS-2/PP blend.

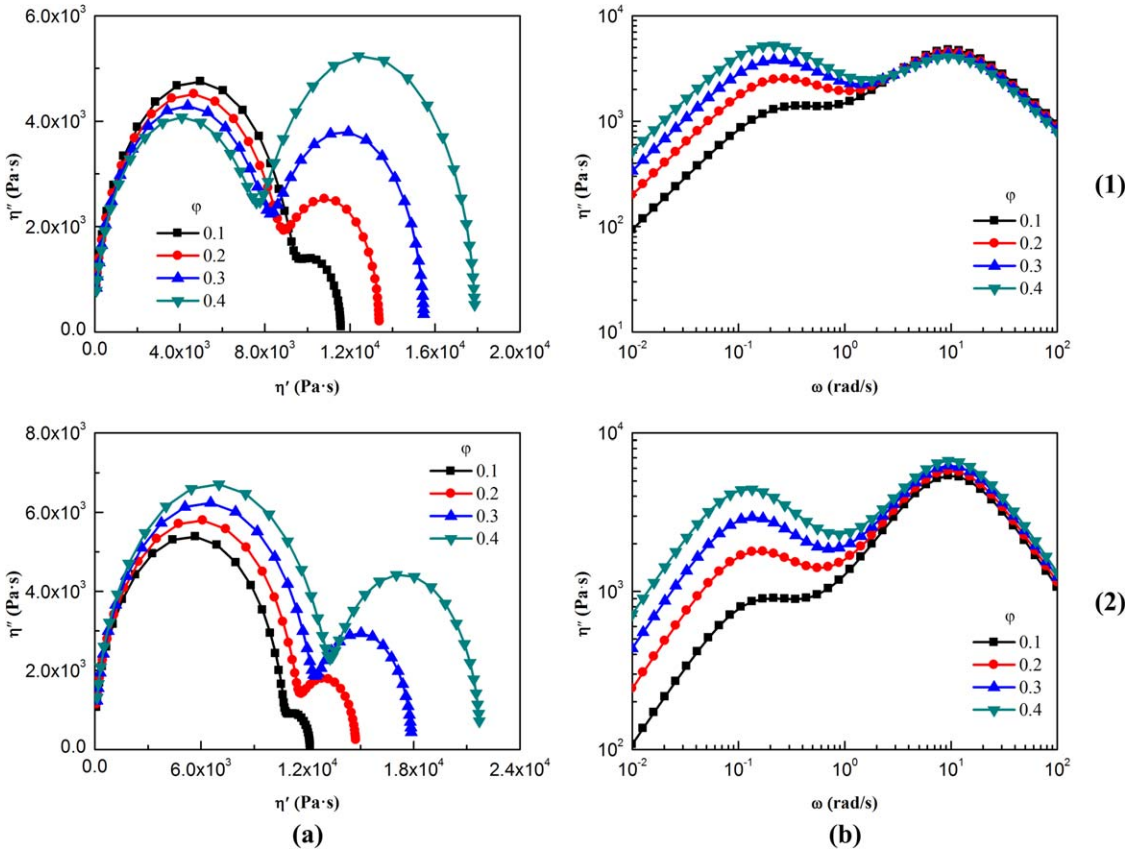

Figure 9. Effect of volume fraction of dispersed phase on (a) Cole–Cole and (b) $\eta''(\omega)$ plots at viscosity ratio of (1) 0.5 and (2) 2.0. [Color figure can be viewed in the online issue, which is available at wileyonlinelibrary.com.]

dispersed droplets, respectively. Increasing the η_i or η_m increases the blend viscosity and thus generates more elastic energy,[21] which increases the radius of the circular arc in the high frequency region. Decreasing the η_i or increasing the η_m leads to the increase in the deformation degree of the dispersed droplets,[21–23] which increases the elastic energy generated by their deformation and thus the radius of the circular arc in the low frequency region, resulting in well separation of the two circular arcs. The aforementioned effect of the η_i was verified by experimental results of the 80/20 (w/w) PLA/PBS-1 and PLA/LLDPE blends with different viscosity ratios (η_r), as shown in Figure 7. From Figure 7(a), compared with the PLA/PBS-1 blend (η_r = 0.19), the PLA/LLDPE blend (η_r = 2.27) exhibits smaller circular arc radius in the low frequency region on the Cole–Cole plot, whereas larger radius in the high frequency region. The Cole–Cole and $\eta''(\omega)$ plots of the 85/15 (w/w) PBS-2/PP blend with a viscosity ratio of 13.1 were calculated to verify the aforementioned effect of the η_m, and the results are shown in Figure 8. From Figure 8(a), there is no peak on the circular arc in the low frequency, which agrees with the predicted result for the blends with low values of the η_m [as shown in Figure 6(a)]. Both predicted and experimental results demonstrate that with increasing the η_i or η_m, the λ_1 increases; the increase in the η_i leads to the increase of the $\lambda_{depression}$, whereas that in the η_m has no effect on the $\lambda_{depression}$, as shown in Figures 5(b), 6(b), and 7(b).

The above results manifest that the λ_m, especially η_i and η_m, play significant roles in the Cole–Cole and $\eta''(\omega)$ plots of the blends. So, the influence of the φ on the two plots is investigated at two viscosity ratios (0.5 and 2.0) while keeping a constant η_m of 10^4 Pa s^{-1}, and the results are shown in Figure 9. As can be seen in Figure 9(a) that with the increase in the φ, the radius of the circular arc in the low frequency region on the

Table IV. Relaxation Times Obtained from $\eta''(\omega)$ Plots for Blends with Different φ

η_r	0.5				2			
φ	0.1	0.2	0.3	0.4	0.1	0.2	0.3	0.4
λ_1 (s)	2.89	3.66	4.64	4.64	4.64	5.88	7.44	7.44
$\lambda_{depression}$ (s)	1.80	0.89	0.70	0.70	—	1.80	1.43	1.13
λ_2 (s)	0.11	0.11	0.11	0.11	0.11	0.11	0.11	0.11

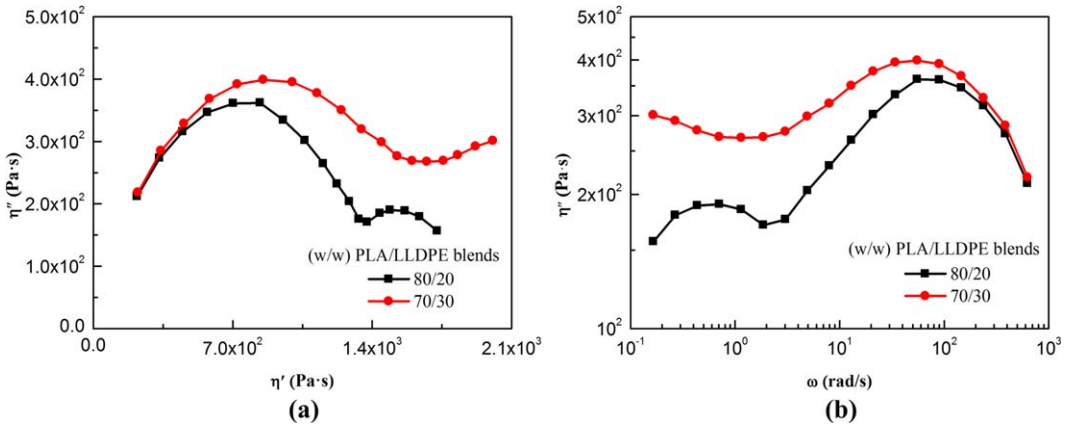

Figure 10. (a) Cole–Cole and (b) $\eta''(\omega)$ plots of as-extruded 70/30 and 80/20 (w/w) PLA/LLDPE blends. [Color figure can be viewed in the online issue, which is available at wileyonlinelibrary.com.]

Cole–Cole plot becomes larger for both viscosity ratios. Moreover, two circular arcs exhibit more distinct separation as the increase in the φ for both viscosity ratios. These are attributed to the fact that higher values of the φ increase the elastic energy generated by the deformation of dispersed droplets. Figure 9(a) also shows that with the increase in the φ, the circular arc in the high frequency region on the Cole–Cole plot exhibits smaller and larger radius for viscosity ratios of 0.5 and 2.0, respectively. It is understandable due to the aforementioned fact that the radius of the circular arc in the high frequency region is mainly affected by the blend viscosity. The relaxation times of the blends obtained from the $\eta''(\omega)$ plots in Figure 9(b) are listed in Table IV. It is clearly seen that λ_1 increases and $\lambda_{depression}$ decreases with the increase in the φ for both viscosity ratios. The Cole–Cole and $\eta''(\omega)$ plots for the 80/20 and 70/30 (w/w) PLA/LLDPE blends with a viscosity ratio of 2.27 were calculated to verify the aforementioned effect of the φ, and the results are shown in Figure 10. As can be clearly seen, both plots for the 80/20 blend present two circular arcs, whereas those for the 70/30 blend only show a tail in the low frequency region, which indicates that the former blend has lower value of the λ_1 than the latter blend. Moreover, the former blend exhibits a smaller radius of the circular arc in the high frequency than the latter blend.

CONCLUSIONS

In the present work, the shape features of the plots of the imaginary part of complex viscosity and the Cole–Cole for the binary immiscible blends were investigated based on the Maxwell and the Palierne models, taking into account of six emulsion parameters: the viscosities and relaxation times of two components, interfacial tension between two components, and volume fraction of the dispersed phase. Moreover, some predicted results were confirmed by the experimental results.

It was found that the peaks in the high- and low-frequency regions on the complex viscosity imaginary part plot are owing to the relaxations of the blend and deformed dispersed droplets, respectively. Higher blend viscosity generates more elastic energy and leads to larger radius of the circular arc in the high frequency region on the Cole–Cole plot. The increases in the matrix viscosity and dispersed phase volume fraction, and the decrease in the dispersed phase viscosity increase the elastic energy generated by the deformation of dispersed droplets, which induce the increase in the radius of the circular arc in the low frequency region and the well separation of the two circular arcs on the Cole–Cole plot. In addition, decreasing the interfacial tension and matrix relaxation time increases the difference of the frequencies corresponding to the two peaks shown on the complex viscosity imaginary part plot, also resulting in well separation of the two circular arcs of the Cole–Cole plot. The λ_1 increases with the increase in the viscosities of two components, especially the decrease in the interfacial tension.

ACKNOWLEDGMENTS

Financial support provided by the National Natural Science Foundation of China (Grant No. 11172105) and Guangdong Provincial Natural Science Foundation (Grant No. S2011010002085) is gratefully acknowledged.

REFERENCES

1. Palierne, J. F. *Rheol. Acta.* **1990**, *29*, 204.
2. Graebling, D.; Muller, R.; Palierne, J. F. *Macromolecules* **1993**, *26*, 320.
3. Calvao, P. S.; Yee, M.; Demarquette, N. R. *Polymer* **2005**, *46*, 2610.
4. Li, R. M.; Yu, W.; Zhou, C. X. *Polym. Bull.* **2006**, *56*, 455.
5. Yokohara, T.; Yamaguchi, M. *Eur. Polym. J.* **2008**, *44*, 677
6. Zhao, Y.; Huang, H. X.; Chen, Y. K. *Polym. Bull.* **2010**, *64*, 291.
7. Peon, J.; Vega, J. F.; Del Amo, B.; Martinez-Salazar, J. *Polymer* **2003**, *44*, 2911.
8. Chopra, D.; Kontopoulou, M.; Vlassopoulos, D.; Hatzikiriakos, S. G. *Rheol. Acta.* **2002**, *41*, 10.
9. Wu, D. F.; Zhang, Y. S.; Zhang, M.; Zhou, W. D. *Eur. Polym. J.* **2008**, *44*, 2171.

10. Wu, D. F.; Zhang, Y. S.; Yuan, L. J.; Zhang, M.; Zhou, W. D. *J. Polym. Sci. Polym. Phys.* **2010**, *48*, 756.
11. Xu, L. Q.; Huang, H. X. *J. Appl. Polym. Sci.* **2012**, *125*, E272.
12. Zhou, Z. Y.; Zhang, Y.; Zhang, Y. X.; Yin, N. W. *J. Polym. Sci. Polym. Phys.* **2008**, *46*, 526.
13. Bai, L.; Li, Y. M.; Yang, W.; Yang, M. B. *J. Appl. Polym. Sci.* **2010**, *118*, 1356.
14. Li, K.; Peng, J.; Turng, L. S.; Huang, H. X. *Adv. Polym. Tech.* **2011**, *30*, 150.
15. Bousmina, M. *Rheol. Acta.* **1999**, *38*, 73.
16. Yu, W.; Zhou, W.; Zhou, C. X. *Polymer* **2010**, *51*, 2091.
17. Ferry, J. D. Viscoelastic Properties of Polymers, 3rd ed.; Wiley: New York, **1980**.
18. Huang, H. X.; Huang, Y. F.; Li, X. J. *Polym. Test* **2007**, *26*, 770.
19. Huang, H. X.; Jiang, G.; Li, X. J. *Int. Polym. Proc.* **2008**, *23*, 47.
20. Li, K.; Huang, H. X.; Jiang, G. *Polym. Plast. Technol. Eng.* **2009**, *48*, 989.
21. Bousmina, M. *Rheol. Acta.* **1999**, *38*, 251.
22. Huang, H. X. *J. Mater. Sci.* **2005**, *40*, 1777.
23. Omonov, T. S.; Harrats, C.; Moldenaers, P.; Groeninckx, G. *Polymer* **2007**, *48*, 5917.